Aging and Disease
www.aginganddisease.org
Volume 15, Number 5; 2255-2270, October 2024
http://dx.doi.org/10.14336/AD.2023.1106

Original Article

Type-2 Diabetes Alters Hippocampal Neural Oscillations and Disrupts Synchrony between the Hippocampus and Cortex

Gratianne Rabiller[1, 2], Zachary Ip[3], Shahram Zarrabian[1, 2], Hongxia Zhang[1, 2], Yoshimichi Sato[1, 2, 4], Azadeh Yazdan-Shahmorad[3, 5], Jialing Liu[1, 2*]

[1]Department of Neurological Surgery, University of California at San Francisco, San Francisco, CA, USA.
[2]San Francisco VA medical Center, San Francisco, CA, USA.
[3]Departments of Bioengineering, University of Washington, Seattle, WA, USA.
[4]Department of Neurosurgery, Tohoku University Graduate School of Medicine, Sendai, Japan.
[5]Electrical and Computer Engineering, University of Washington, Seattle, WA, USA.

[Received September 6, 2023; Revised November 3, 2023; Accepted November 6, 2023]

ABSTRACT: Type 2 diabetes mellitus (T2DM) increases the risk of neurological diseases, yet how brain oscillations change as age and T2DM interact is not well characterized. To delineate the age and diabetic effect on neurophysiology, we recorded local field potentials with multichannel electrodes spanning the somatosensory cortex and hippocampus (HPC) under urethane anesthesia in diabetic and normoglycemic control mice, at 200 and 400 days of age. We analyzed the signal power of brain oscillations, brain state, sharp wave associate ripples (SPW-Rs), and functional connectivity between the cortex and HPC. We found that while both age and T2DM were correlated with a breakdown in long-range functional connectivity and reduced neurogenesis in the dentate gyrus and subventricular zone, T2DM further slowed brain oscillations and reduced theta-gamma coupling. Age and T2DM also prolonged the duration of SPW-Rs and increased gamma power during SPW-R phase. Our results have identified potential electrophysiological substrates of hippocampal changes associated with T2DM and age. The perturbed brain oscillation features and diminished neurogenesis may underlie T2DM-accelerated cognitive impairment.

Key words: Local field potential, T/D, modulation index, phase locking index, coherence, sharp wave associated ripples, neurogenesis

INTRODUCTION

The global prevalence of type 2 diabetes mellitus (T2DM) is on the rise [1], with over half a billion people already affected in 2018. T2DM is also a significant risk factor for a wide spectrum of neurological diseases including ischemic stroke, depression, and the Alzheimer's disease (AD) [2]. T2DM accelerates normal brain aging by increasing gray matter atrophy 26% ± 14% faster than seen with normal aging, thus T2DM patients displayed a more rapid rate of cognitive decline than typically associated with natural aging [3]. As such, T2DM potentiates the development of dementia [4].

Like age, diabetes has complex and profound effects on brain volume, neural activity, functional connectivity and cognitive function [5-7]. However, how T2DM and age interact to cause structural and network changes that may underlie cognitive dysfunction remains unclear. In humans, T2DM causes EEG rhythms to shift from higher to lower frequencies and reduces neural synchrony albeit to a lesser extent compared to other pathological cognitive aging disorders such as AD [8, 9]. Experimental models

***Correspondence should be addressed to:** Dr. Jialing Liu, Department of Neurological Surgery (112C), University of California at San Francisco and Department of Veterans Affairs Medical Center, San Francisco, California 94158, USA. Email: jialing.liu@ucsf.edu.

using invasive recording modalities to probe deeper brain regions like the hippocampus (HPC) offer better opportunity to decipher the neurophysiological outcome of age and T2DM in learning and memory, circumventing the difficulty in assessing cognitive behavior in the T2DM models [10].

Recent evidence suggests that neurogenesis might compensate for the age-associated hyperexcitability of the CA3 area via a feed-forward inhibition mechanism [11], supported by evidence of direct contact between the filopodia of the mossy fiber terminals of the new neurons and parvalbumin interneurons [12, 13]. Increasing neurogenesis via overexpression of the cell cycle regulators CDk4/cyclinD1 not only rescued degraded navigational strategy and improved memory performance in the aged mice, but also restored the profile of hippocampal sharp wave associated ripples (SPW-Rs) [11], a CA1 specific brain oscillation known to underlie memory consolidation. These findings suggest that reduced neurogenesis has a causal role in altering hippocampal trisynaptic circuitry, resulting in perturbed brain oscillations. Yet the role of T2DM in accelerating age induced reduction in neurogenesis and the extent in disturbing brain oscillations has not been established.

To test the hypothesis that T2DM-induced brain atrophy may alter connectivity between cortex and brain regions crucial for memory, we recorded field potentials in the sensorimotor cortex and HPC in two age groups of diabetic and normoglycemic mice under urethane anesthesia. We found that both aging and T2DM disrupted functional connectivity between the cortex and HPC and led to increase in the duration of SPW-Rs, and gamma power during SPW-Rs. These changes were associated with reduced neurogenesis in the HPC. However, compared to the impact of aging, T2DM additionally caused increased slowing scores and reduced aperiodic spectral exponent in the HPC. These results suggest that T2DM has a unique impact on brain oscillations and functional connectivity, beyond the effects of aging alone. The combination of these changes may contribute to the accelerated cognitive decline seen in older individuals with T2DM.

MATERIALS & METHODS

Animals and housing

Diabetic db/db mice (B6.BKS(D)-Lepr<db/db>/J) homozygous for the leptin receptor gene mutation were used as the model of obesity-induced T2DM, while heterozygous db/+ mice (B6.BKS(D)-Lepr<db/+>/J) were used as normoglycemic controls [14-16]. Male and female db/+ and db/db mice at 200 or 400 days of age were housed in the institutional standard cages (5 mice per cage) on a 12-h light/12-h dark cycle, with ad libitum access to water and food. All animal experiments were conducted in accordance with the Guide for Care and Use of Laboratory Animals issued by the National Institutes of Health and approved by San Francisco Veterans Affairs Medical Center Institutional Animal Care and Use Committee. The identity of each mouse subject was blinded to investigators who conducted the experiments and data analysis.

Electrophysiological recording

Recordings were performed using 16-channel extracellular silicon electrodes (A1x16-5mm-100-703, NeuroNexus Technologies) under urethane anesthesia (Sigma, 1 g/kg i.p.) for one hour [17, 18]. Following craniotomy and resection of the dura mater, 2 electrodes were each inserted into left and right hemispheres to target the dorsal HPC at [AP: -1.84 mm; ML: +/- 1.2 mm; DV: 1.4] via a stereotaxic frame (David Kopf Instruments, Tujunga, CA, USA). Real-time data display and an audio aid were used to facilitate the identification of proper recording locations while advancing electrodes until characteristic signals from stratum pyramidale and stratum radiatum were detected and recorded [17]. A 1-hr multi-channel recording from bilateral sensorimotor cortex and dorsal HPC was collected from each mouse. Data were stored at a sampling rate of 32 kHz after band-pass filtering (0.1-9 kHz) with an input range of ± 3 mV (Digital Lynx SX, Neuralynx, USA). Data were down sampled to 1250 Hz for further analysis. A total of 23 mice were successfully recorded and subjected to data processing. The groups had the following counts: db/+ 200 d (n = 7), db/db 200 d (n = 6), db/+ 400 d (n = 5), db/db 400 d (n = 5). Mortality rate was about 15% due to reaction to urethane anesthesia.

Electrophysiology data analysis

Spectral power analysis: Local field potentials from the pyramidal layer and stratum lacunosum moleculare (slm) of the HPC and the deep cortical layer of the sensorimotor cortex were used in our analysis. Brain waves were filtered from the LFPs according to the following frequency ranges: delta (0.1–3 Hz), theta (4–7 Hz), gamma (30–58 Hz), and high-gamma (62–200 Hz) and signal power determined as previously described [17]. A slowing score was calculated, defined as the ratio between low frequency (1-8 Hz) and high frequency oscillations (9-30 Hz), where higher values of the slowing score correspond to a shift in spectral power from high to low frequencies [19]. Theta state in the brain was determined by calculating the ratio of theta/delta (T/D) Hilbert amplitudes in the slm layer of the HPC. The amplitude

envelopes were smoothed with a Gaussian kernel (σ = 1 s, 8 s window), and the T/D was further smoothed with a second Gaussian kernel (σ = 10 s, 80 s window), to stabilize changes of state and reduce noise. The smoothed ratio was then split by a manual threshold set by visual assessment to define two states, high theta/delta (HT/D) and low theta/delta (LT/D) [20-22].

Estimation of the spectral exponent from the PSD background: Since changes in spectral power can be reflected by both periodic and aperiodic components, we also quantified the latter. Isolated from the aperiodic component of the signal as described previously [23], the spectral exponent (SE) measures the steepness of the decay of the power spectral density (PSD) background [24]. PSD is assumed to decay according to the inverse power- law $\sim 1/f^{\alpha}$, therefor we define the SE to be $\beta = -\alpha$. The SE therefore is equivalent to the slope of the linear regression resulting from the log of the PSD [25]. We estimated the PSD using Welch's method (2s window, 50% overlap) and SE calculated between the 1-40 Hz range.

SPW-Rs detection and characterization: SPW-Rs were identified from the pyramidal layer during LT/D periods [18]. To isolate SPW-Rs, the LFP signal of the pyramidal layer was filtered (150–250 Hz), squared, and Z-scored. When the signal exceeded 4 standard deviations for a period longer than 0.05 msec, a SPW-R event was registered. When the signal subsequently dropped below 1 standard deviations, the event was considered to have ended. Multiple characteristics of SPW-Rs were calculated. Duration and inter-ripple interval (IRI) were calculated using the start and end timings of SPW-R events.

Pyramidal gamma LFP power during SPW-Rs: SPW-R-associated slow gamma signal power was calculated using the averaged z-scored power over the 30–50 Hz frequency band 0–100 msec after ripple detection. This was then averaged over all SPW-RS events.

Functional connectivity: Functional connectivity between the cortex and HPC areas was estimated using three methods; i.e. Phase locking index (PLI), coherence, and cross regional phase amplitude coupling (xPAC).

Phase locking Index (PLI): An index of asymmetry of the distribution of phase differences between measured signals was calculated [26, 27]. PLI is a measure of the consistency in the distribution of instantaneous phase differences between two signals. If the phase differences between two time series are $\triangle\phi(t\_k)(k = 1 \ldots N)$, PLI is defined as:

$$PLI = |\langle sign[\triangle\phi(t\_k)]\rangle|$$

where $\langle\cdot\rangle$ is the mean value operator. PLI values range from 0 - 1, where a value of 0 indicates no coupling or coupling with a phase difference centered around 0 mod pi, and a value of 1 reflects complete synchrony between two signals. PLI was computed for the following frequency bands: delta (0.1-3 Hz), theta (4-7 Hz), alpha (8-13 Hz), beta (13-30 Hz), gamma (30-58 Hz), and high gamma (62-200 Hz).

Coherence: Coherence measures the consistency of a phase relationship between two signals. Coherence was calculated pairwise between cortex, CA1 pyramidal, and CA1 slm layer of the HPC for each of the frequency bands. The coherence between signals x and y is defined as the square of the cross-spectrum of the channels divided by the product of the power spectra of the individual channels:

$$C_{xy}(f) = \frac{|G_{xy}(f)|^2}{G_{xx}(f)G_{yy}(f)}$$

where Gxx and Gyy refer to power spectral density of channels x and y respectively, and Gxy refers to their cross-spectral density [28].

Cross-regional phase-amplitude coupling (xPAC): xPAC was measured between the pyramidal layer and the cortex as described previously [17, 18]. To estimate xPAC we bandpass-filtered the LFP between 0.1 and 200 Hz, extracted the instantaneous phase from the pyramidal layer and instantaneous amplitude from the cortical layer using the Hilbert transform. A composite phase-amplitude time series then determined the amplitude distribution across phase. The modulation index (MI) was then calculated from the divergence of the amplitude distribution from a uniform distribution [29]. MI was compared between groups by averaging the MI across a window of frequencies pertaining to canonical frequency bands. A data driven threshold was found using Otsu's method [30] to determine the window of significant coupling.

In vivo labeling by 5-bromo-2'-deoxyuridine-5'-monophosphate (BrdU)

To track cell proliferation, BrdU (Sigma-Aldrich, MO, USA) was administered intraperitoneally (i.p.; 50 mg/kg; two times per day for a period of 4 days) to the db/db and db/+ mice as described previously [31]. To enhance the detection rate of colocalization between BrdU and cell type specific markers, the dose of BrdU was increased to 75 mg/kg and three times daily for a period of 4 days in the 200-day groups. Mice were euthanized 2-3 weeks after BrdU administration.

Brain dissection and tissue processing

Prior to the brain dissection, adult mice were anesthetized with isoflurane (2-5% with 30-40% O2 and 60-70% nitrous oxide in gas), and intracardially perfused with 300 ml of 4% paraformaldehyde (PFA). The brains were

extracted and post fixed in 4% PFA overnight at 4 °C. Following cryoprotection in 20% sucrose, 40 µm-thick coronal sections were cut on a freezing microtome and collected serially [32].

Immunocytochemistry and immunofluorescence staining

Immunohistochemistry of dentate gyrus (DG) and subventricular zone (SVZ) regions was performed on 40-µm serial free-floating sections. To improve the efficiency of BrdU detection, sections were pretreated with 1 N HCl for 30 min and then neutralized with 0.1 M sodium borate buffer pH 8.5 for 10 min prior to incubation with primary antibody. Sections were blocked and permeabilized with blocking serum (0.3% Triton X-100, 2% BSA, and 1% donkey serum) for 30 minutes, followed by incubation in mouse anti-BrdU (1:400, Cat#:11170376001, Roche, Basal, Switzerland), goat anti-DCX (1:1000, clone C18, sc-8066, Santa Cruz Biotechnology, TX, USA), mouse anti-NeuN (1:1000, MAB377, Millipore, MA, USA) and rabbit anti-GFAP (1:500, Z0334, Dako, CA, USA) overnight at room temperature and then with donkey anti-mouse (Cat#715-545-150), anti-goat (Cat#705-585-147), or anti-rabbit (Cat#711-585-152) secondary antibodies conjugated to Alexa 488 or 594 (1:400, Jackson ImmunoResearch, West Grove, PA, USA) for 2 hours at room temperature according to the methods described previously [31, 33]. For DAB staining, donkey anti-goat (Cat#705-065-147) or anti-mouse (Cat#715-065-151) biotinylated secondary antibodies were incubated for 2 hours at room temperature (1:1000, Jackson ImmunoResearch, West Grove, PA, USA), followed by incubation with VECTASTAIN Elite ABC HRP solution (Vector, CA, USA) for 1.5 hour at room temperature. The substrate response was detected with DAB (Sigma-Aldrich, MO, USA) until satisfactory brown staining was achieved. The sections were then dehydrated in ascending concentrations of alcohol, cleared in Citrisolv, mounted with permanent mounting medium as previously described [34].

Imaging and quantification

Fluorescence signals were detected by using the Zeiss Spinning Disk confocal image system (Zeiss, Thornwood, NY) using a sequential scanning model with step size of 1 µm for Alexa 488 and 594. Images were processed by Zeiss ZEN software for orthogonal and maximal intensity projection. Montages were created by Adobe Photoshop (Adobe System, Mountain View, CA). DAB or cresyl violet (CV) signals were captured with a CCD camera attached to Zeiss Axio II microscope equipped with StereoInvestigator software (MicroBrightField, VT, USA).

Quantification of CV and DAB staining of DCX or BrdU in SVZ was performed as previously described [35]. Images were digitally captured under a 10X objective and imported into Image J (NIH) for analysis. The area of DCX or progenitor cell staining in dorsolateral SVZ in DAB and CV staining were outlined and calculated. The average cell count, or area were averaged from 3 sections of SVZ and DG each per mouse at the same AP levels. DG cell counts were adjusted to represent the entire HPC by multiplying the total number of sections.

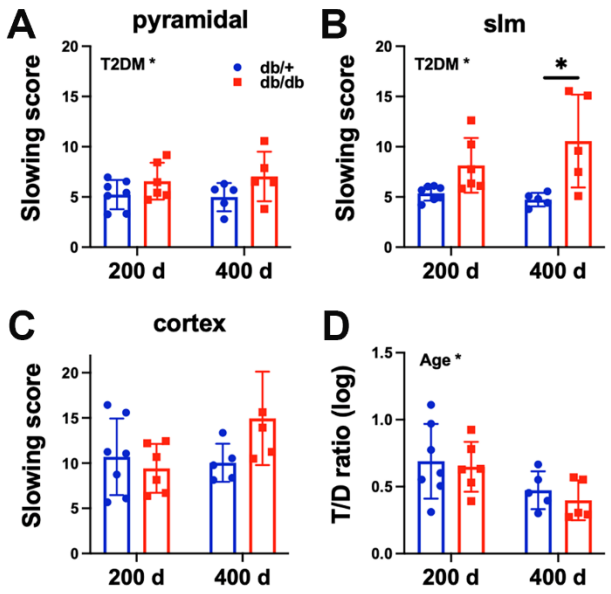

Figure 1. T2DM increased slowing score in the hippocampus (HPC) and age altered brain state. Slowing score of the pyramidal **(A)**, slm **(B)** layers of the hippocampus and cortex **(C)**. T2DM mice shifted the power towards lower frequency oscillations in comparison to the control mice in the pyramidal and slm layers of the HPC. **(D)** Age altered brain state by reducing theta/delta (T/D) ratio. Two-way ANOVA test followed by Tukey's post-hoc test. 200 d: 200 days old, 400 d: 400 days old. *p < 0.05, ***p < 0.001.

Statistical analysis

Data were expressed as mean ± standard deviation in all figures and checked for normal distribution using the Kolmogorov-Smirnov or Shapiro-Wilk normality test. We used two-way analysis of variance (ANOVA) to assess the genotype and age effects and their interaction. We first tested for interaction and, when it was not statistically significant, we dropped it from the model to interpret the main effects of age and genotype. We also conducted pairwise comparisons of the age effect (within genotype) and the genotype effect (within ages). As a sensitivity analysis we used a non-parametric bootstrap to

verify our results in case the data were not normally distributed [36] (using SAS package). Adjusted p values less than 0.05 were considered as significant.

RESULTS

T2DM slowed neural rhythms in the HPC while age reduced T/D ratio

We assessed the slowing score, defined by the ratio of signal power of low frequencies (1-8 Hz) over high frequency oscillations (9-30 Hz) within the cortex or HPC. We found that T2DM was associated with significantly increased slowing score in both pyramidal ($p < 0.05$) and slm ($p < 0.001$) layers of the HPC (Fig. 1A). With respect to the effect on individual frequency band, T2DM had a tendency to lower signal power of higher frequency oscillations (not shown). Regarding brain state, age significantly decreased the ratio of HT/D to LT/D ($p < 0.05$), indicating that age reduced time spent in HT/D (Fig. 1B).

The spectral exponent of the aperiodic signal

We next analyzed the power spectral density and aperiodic signals of the field potentials. T2DM exponentially reduced power with increasing frequency in the slm layer of the HPC, reflecting a diabetes-associated increase in spectral exponent due to a faster decay of high frequency signal power in the HPC, which was more prominent in the older group (Fig. 2).

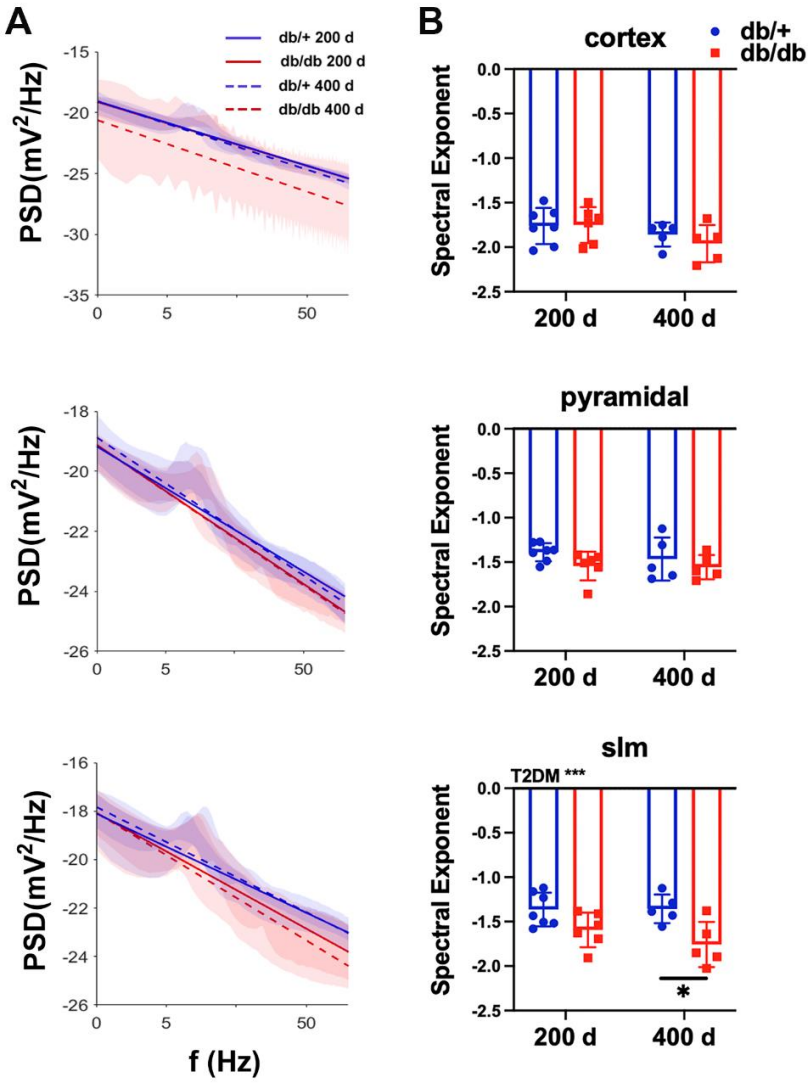

Figure 2. T2DM reduced spectral exponent in the slm layer of the HPC. (A) Average power spectral density of recordings and best-fit trendline for each group. **(B)** Comparison of the spectral exponent showing the older T2DM mice had the most reduced spectral exponent. Two-way ANOVA test followed by Tukey's post-hoc test. 200 d: 200 days old, 400 d: 400 days old. *$p < 0.05$, ***$p < 0.001$.

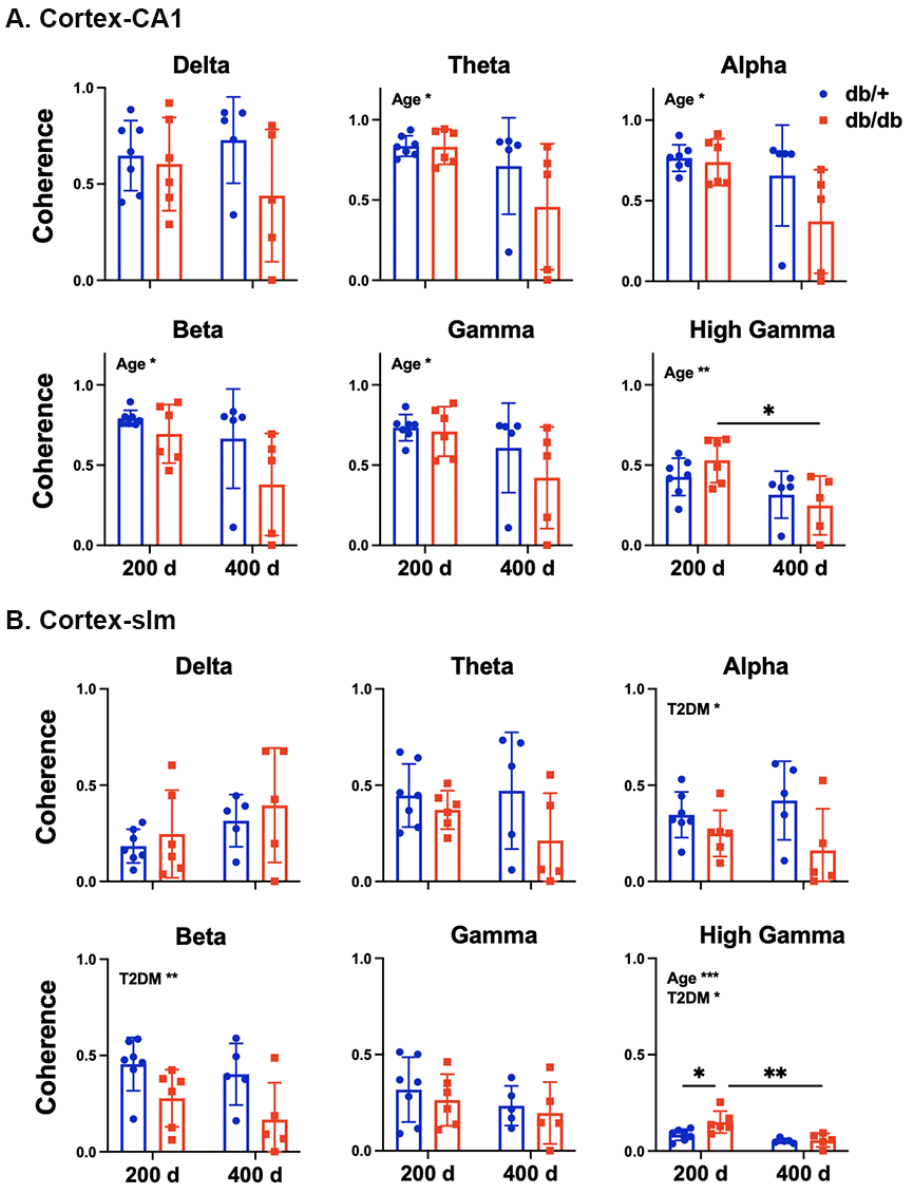

Figure 3. Age and T2DM reduced coherence at a number of frequency bands between cortex and HPC. (A) Cortex- pyramidal coherence: Age decreased coherency between the cortex and pyramidal layer in all but delta frequency. **(B)** Cortex-slm coherence: T2DM effect in reducing coherency was observed in alpha, beta, and high gamma frequency bands. Two-way ANOVA test followed by Tukey's post-hoc test. 200 d: 200 days old, 400 d: 400 days old. *p < 0.05, **p < 0.01, ***p < 0.001.

Age and T2DM reduced cortico-hippocampal coherence and phase synchrony

We determined functional connectivity between brain networks in the frequency domain by coherence and phase synchrony. By measuring the consistency of relative amplitude and phase between signals detected in two regions within a set of frequency band, we found that coherence significantly decreased as a function of age between cortex and CA1 in theta, alpha, beta, gamma (Two way ANOVA, age effect: $p<0.05$), and high gamma (age effect: $p<0.01$) frequency bands (Fig. 3A). Meanwhile, coherence reduced as a function of T2DM in alpha (T2DM effect: $p < 0.05$), beta (T2DM effect: $p < 0.001$), and high gamma (T2DM effect: $p < 0.05$) frequency bands between cortex and slm layer (Fig. 3B). By measuring how stable the phase difference varies over a period of time between two regions independent of the amplitude of oscillations, we found that the phase synchrony represented as PLI decreased as a function of

age in theta, alpha, beta, gamma, and high gamma frequencies between cortex and CA1 (age effect: $p<0.05$) in a consistent manner as in coherence, in addition to the T2DM associated decrease in delta frequency (T2DM effect: $p<0.05$) (Fig. 4A). PLI also decreased as a function of T2DM in beta and gamma (T2DM effect: $p<0.05$) frequencies between cortex and slm layer (Fig. 4B). Our data suggest that both age and T2DM decreased functional connectivity between cortex and HPC.

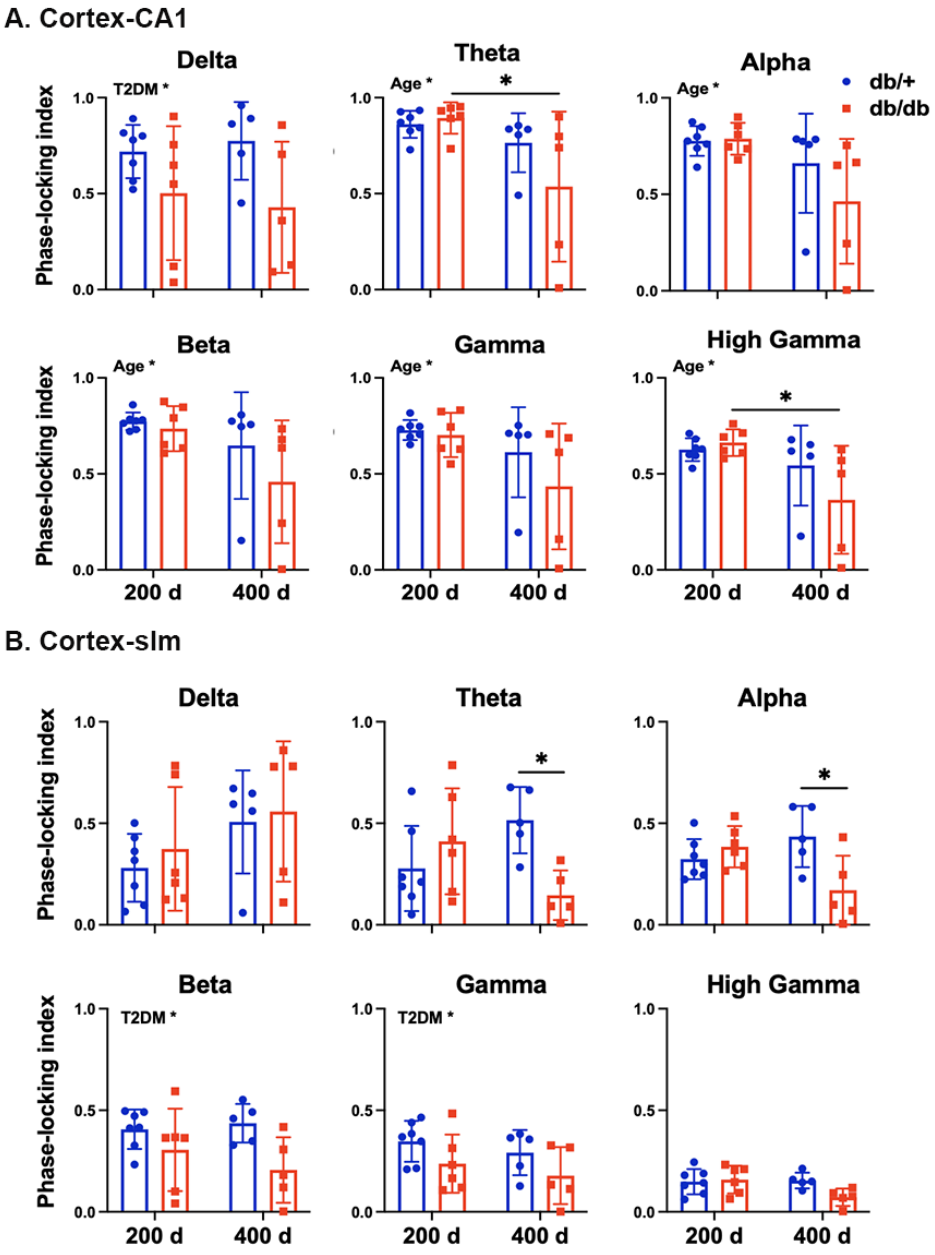

Figure 4. Phase locking index (PLI) quantification for individual frequency bands between (A) cortex and pyramidal and (B) cortex and slm layers. Age significantly decreases PLI between the cortex and pyramidal layer in all frequency bands except delta frequency. T2DM decreased PLI between cortex and pyramidal layer in delta and between cortex and slm layer in theta, beta, and gamma bands. Two-way ANOVA test followed by Tukey's post-hoc test. 200 d: 200 days old, 400 d: 400 days old. *$p < 0.05$.

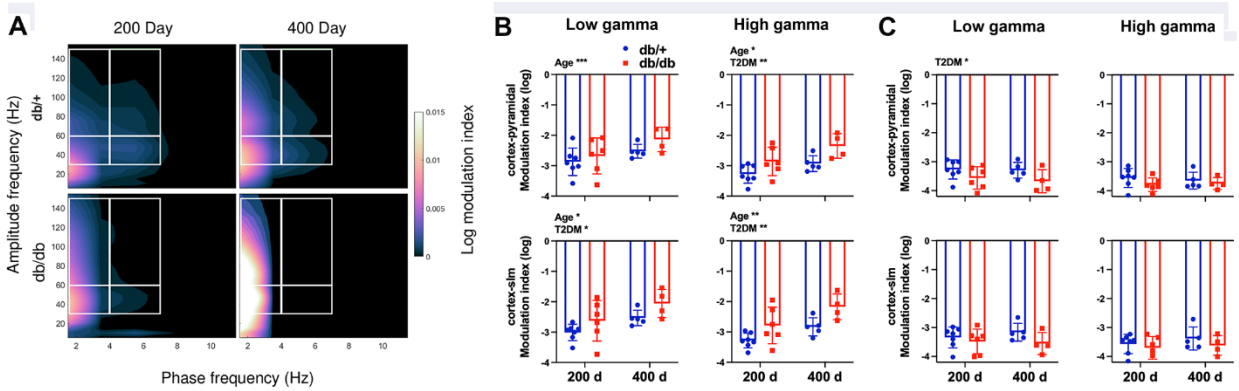

Figure 5. Cross regional phase-amplitude coupling between cortex and pyramidal or slm layer of the HPC. (A) Comodulograms of cortex-pyramidal areas demonstrating delta-high gamma (upper left), theta-high gamma (upper right), delta-low gamma (lower left), and theta low-gamma (lower right) coupling area marked by white boxes. **(B)** Quantified average log modulation index (MI) within areas of interest. Age or T2DM increased MI between delta and gamma, while T2DM reduced MI between theta and gamma. Two-way ANOVA test followed by Tukey's post-hoc test. 200 d: 200 days old, 400 d: 400 days old. *p < 0.05, **p < 0.01.

Both age and T2DM showed dynamic effects on cross regional phase-amplitude modulation between cortex and HPC

A third approach to assess functional connectivity is via cross regional phase-amplitude relationship in different frequency bands between cortex and pyramidal or slm layers of the HPC using phase-amplitude coupling analysis. We found that both age and T2DM increased delta-gamma phase-amplitude coupling between the HPC and cortex as shown by the MI, while T2DM decreased theta-gamma coupling (Fig. 5). Our data suggest that T2DM led to disrupted communication between cortico-hippocampal circuits.

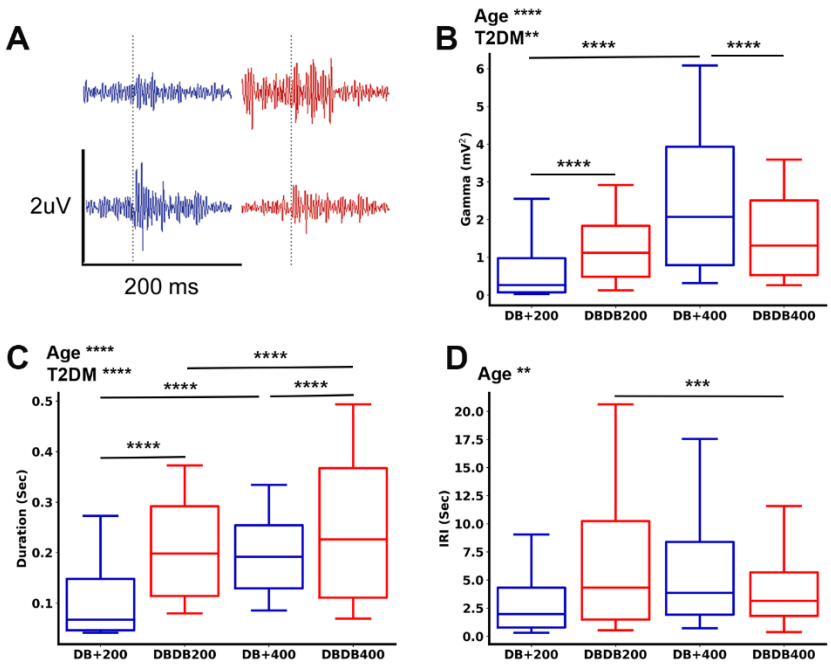

Figure 6. Characteristics of sharp wave associate ripples (SPW-Rs). (A) Average ripple waveform in 200 msec clips. **(B-D)** box-whisker plots of the 10-90% quantile comparing gamma signal power during SPW-Rs (B) and duration of SPW-Rs (C). Age and T2DM increased ripple duration and gamma power during ripples. **(D)** Comparison of inter-ripple intervals (IRI). Age significantly reduced IRI and this reduction was especially prominent in T2DM mice. Two-way ANOVA test followed by Tukey's post-hoc test. 200 d: 200 days old, 400 d: 400 days old. An average of 1190 ripples were analyzed per group. **p < 0.01, ***p < 0.001, ****p < 0.0001.

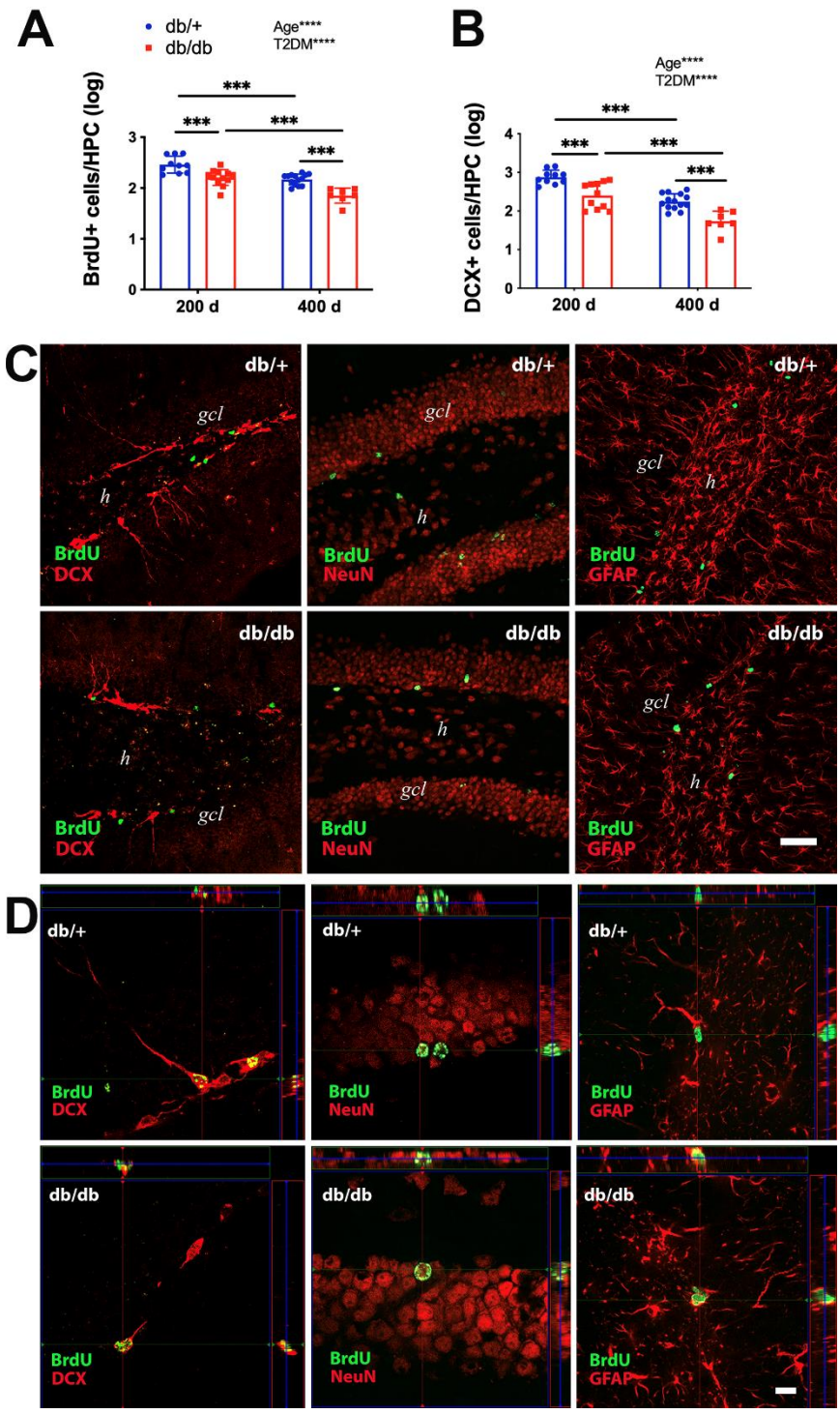

Figure 7. Age and diabetes reduced cell proliferation and immature neurons in the dentate gyrus subgranular zone (SGZ). The numbers of proliferating neural progenitor cells and neuroblasts in the SGZ of the HPC were quantified using BrdU **(A)** and double cortin (DCX) staining **(B)**. Two-way ANOVA test followed by Tukey's post-hoc test showed significant effect of age and T2DM on hippocampal neurogenesis. 200 d: 200 days old, 400 d: 400 days old. ***p < 0.001, and ****p < 0.0001. **(C)** Representative double immuno-fluorescent staining of the dentate gyrus in lower magnification (20X) view from 200-day old db/+ (upper panel) and db/db (lower panel) for BrdU (green) and DCX, NeuN or GFAP (red). gcl: granule cell layer. h: hilus. Scale bar, 50 µm. **(D)** Orthogonal reconstructions of confocal microscope merged images from db/+ (upper panel) and db/db (lower panel) with BrdU as green and cell markers (DCX, NeuN or GFAP) as red as viewed in the x–z (top) and y–z (right) planes. Scale bar, 10 µm. Group sizes for 200d: 10/db/+, 11/dbdb; 400d: 14/db+, 7/dbdb.

Age and T2DM affected the duration of SPW-Rs and gamma power during SPW-Rs

We next examined how age or T2DM affected the properties and emergence of SPW-R, a hippocampal specific oscillation resulting from the dynamical interaction between pyramidal cells and GABAergic interneurons within the local hippocampal circuits. We first examined the amount of network activation in CA1 during SPW-Rs by measuring gamma signal power (Fig. 6B). We found that both age and T2DM increased gamma power during SPW-Rs firing (Fig. 6B). We then found

that both age and T2DM prolonged ripple duration ($p < 0.0001$; Fig. 6C). Specifically, older db/db mice had reduced IRI (Fig. 6D) compared to younger ones, likely due to increased ripple duration. The longer ripples and increased gamma power suggest that age and T2DM likely increased the excitability of the HPC.

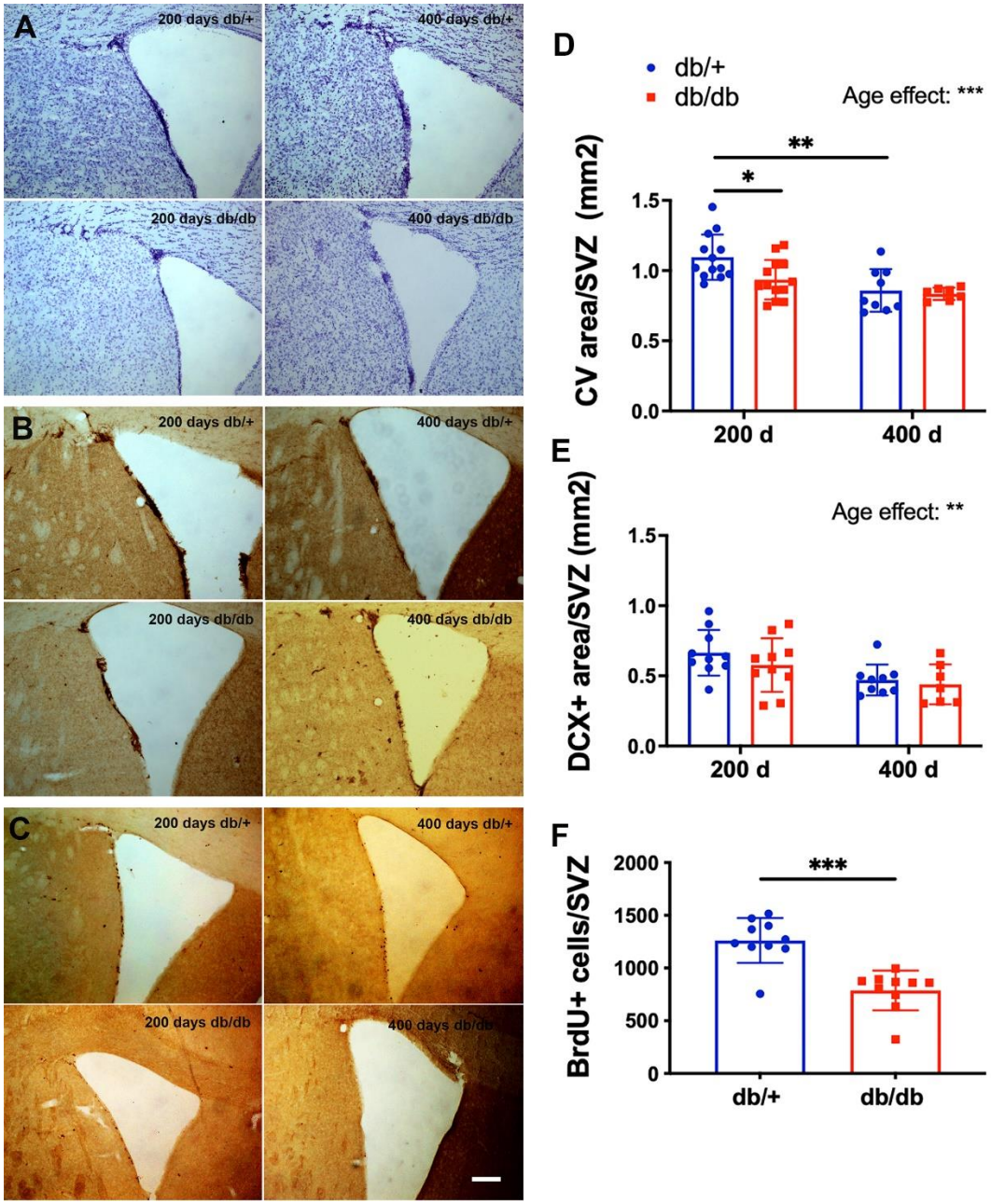

Figure 8. Age reduced progenitor cell activity in the subventricular zone (SVZ). The number of proliferating neural progenitor cells and neuroblasts in the SVZ was quantified using Cresyl violet (CV) staining **(A, D)** DCX staining **(B, E)** and BrdU staining **(C, F).** Representative images (A-C) from each group showed the regions in the SVZ and lateral ventricle where neuroprogenitor cells and neuroblasts reside. Scale bar, 100 µm. BrdU counts were not shown for the 400 d groups due to very low numbers were found **(F)**. There was an overall effect of age on neuroprogenitor cells and immature neurons, while T2DM reduced neuroprogenitor cells and cell proliferation in the 200 d group. Two-way ANOVA test followed by Tukey's post-hoc test. *$p < 0.05$, **$p < 0.01$, and ***$p < 0.001$. 200 d: 200 days old, 400 d: 400 days old. Group sizes for 200 d: 10-13/db/+, 10-13/dbdb; 400 d: 9/db+, 7/dbdb.

Both age and T2DM decreased neurogenesis in the HPC

To determine how T2DM interacts with age to affect neural stem cell activity, we quantified the levels of neurogenesis in the SGZ of the dentate gyrus and the subventricular zone (SVZ). We found that both age and T2DM were associated with significant decreases in cell proliferation ($p < 0.0001$; Fig. 7A) and the total number of DCX(+)-neuroblasts in the SGZ ($p < 0.0001$; Fig. 7B). Newborn cells from 200-day control and diabetic mice developed into neurons and astroglia in the dentate gyrus 2-4 weeks after the division of progenitor cells (Fig 7C, D). There was also a significant age-associated reduction in neurogenesis in the SVZ ($p < 0.01$; Fig. 8).

DISCUSSION

While systematic changes in neural oscillations are known to occur under normal and pathological aging [37-42], how cognitive aging risk factors alter or accelerate these natural progressions is unclear. Here, we investigated the effect of T2DM and aging on neural oscillations in the HPC and neural synchrony between brain regions. We found that age strongly reduced theta brain state, while T2DM significantly increased slowing score and reduced the spectral exponent of the aperiodic signal in the HPC. Age and T2DM both increased SPW-Rs duration and gamma power during ripple firing. With respect to neural synchrony, age and T2DM reduced PLI and coherence between cortex and HPC in various frequencies. Most importantly, both age and T2DM increased delta-gamma coupling while T2DM reduced theta-gamma coupling between HPC and cortex. Although T2DM is widely accepted as an accelerated aging with known effect on cortical atrophy, we report here for the first time that the electrophysiological manifestation of T2DM is more prominent in the HPC as reflected by the increased SPW-Rs and slowing score as well as reduced neural synchrony between cortex and HPC.

Reduced amplitude and peak frequency of the alpha-band was often reported during normal cognitive aging in humans [38, 43, 44], whereas our study in mice showed a consistent age effect on diminishing signal power in theta and alpha bands in the cortex. Compared to age effect, T2DM significantly increased slowing score and decreased signal power in the beta frequency range in the HPC. In addition to changes often reported in the periodic component, recent work has suggested that the aperiodic component of LFP signals contains physiologically relevant information that changes with age and cognitive functions [45]. Our data in T2DM-associated steepening in the spectral exponent of the aperiodic signal implies a tilted balance of synaptic excitation and inhibition [46, 47]. Apart from weakening oscillation power, we found that age also altered brain state by proportionally prolonging the LT/D periods, and in turn shortening HT/D periods. The balance and duration of brain states has been shown to be essential to proper memory function [48], and thus an altered brain state may be an indicator of disrupted learning, memory, and cognitive functions.

As one of the electrophysiological proxies of functional connectivity between brain regions, PLI measures neuronal synchrony between two recorded signals. A reduction in PLI globally across the neocortex has been reported in T2DM [49] and mild cognitive impairment [50, 51]. In our study we have also detected a decrease in PLI between cortex and HPC over various frequency bands as a function of T2DM or age, showing that the decrease in PLI extends to connections between the neocortex and the temporal lobe in diabetic or aged mice. Unlike PLI which measures the consistency of the instantaneous phase difference between two signals, coherence determines the ratio of the cross spectral density and the individual auto spectral densities albeit with a lower temporal specificity. Coherence has been shown to be altered by neurological disorders such as stroke [52], depression [53, 54], AD [55], Down syndrome with AD [56], and aging [57]. Similar to the PLI, we detected a decrease in coherence due to age or diabetes. Theta oscillations in the HPC provide a temporal reference for gamma oscillations through theta-gamma coupling [58]. Consistent with recent work revealing that the HPC and cortical areas utilize xPAC to support memory encoding [59], our data showed that theta-gamma xPAC was reduced between cortex and HPC by T2DM, similar to the effect of chronic ischemic stroke in rats [18]. Our findings in T2DM associated reduction in functional connectivity in mice assessed by electrophysiology is in line with the fMRI findings showing decreased functional connectivity in the hippocampus of human T2DM patients [6, 7, 60, 61].

SPW-Rs are among the most synchronous spontaneous population patterns in the mammalian brain, and recent evidence suggest that these waves serve to reactivate neurons encoding episodic memories to promote memory consolidation and also contribute to the planning of future actions by generating ordered neuronal firing sequences [58, 62, 63]. SPW-Rs may be phase-coupled with a power spectral peak in the slow gamma band originating from the CA3, which in turn determines information flow in the HPC-EC system [64]. Thus, disruption of SPW-Rs and/or gamma oscillation in the HPC-EC of experimental animals and humans causes severe memory impairment [65-70]. For the first time our study has revealed that age and T2DM increase the duration of hippocampal SPW-Rs and gamma power during SPW-Rs, while age reduce inter-ripple interval.

The increased gamma power during SPW-Rs suggests that neurons firing during SPW-Rs become more excitable as a function of age or T2DM.

Our finding in age- and T2DM-associated reduction in hippocampal neurogenesis and changes in SPW-Rs characteristics is consistent with the physiological role of hippocampal neurogenesis in maintaining the balance of excitatory and inhibitory activity and proper cognitive function. Established evidence suggests that newborn neurons project monosynaptic inhibitory input onto granule cells, producing a feed-forward inhibition of CA3 neurons [71]. This process is crucial in maintaining remote memory [47], but is weakened by age [72], resulting in hyperexcitability of the CA3 auto-associative network that has been proposed to lead to memory rigidity during aging [12, 13]. Increased neurogenesis by Cdk4/cyclinD1 overexpression triggered an overall inhibitory effect on the trisynaptic hippocampal circuit and reversed age-associated CA3 hyperactivation, resulting in decreased occurrence, duration and increased interval of SPW-Rs [11]. However, our findings might not seem intuitively compatible with an earlier study showing that the longer duration of ripples was found to be related to mnemonic demand and performance [65]. A few factors might have contributed to the seemly discrepant findings between the two studies. First, the main difference is that the SPW-Rs detected in our study are not task dependent. Second, the average duration of SPW-Rs detected in our T2DM or older mice was more than 250 msec, which was significantly longer than the physiological ripples ranging 1-200 msec. Longer ripples likely reflect the pathological condition of the HPC and differ from physiological ripples in their involvement in memory function. In the condition of traumatic brain injury, the resulting deafferentation was reported to induce hyperexcitability of distal dendrites in the hippocampal pyramidal neurons [73]. Consistent with this notion, longer duration of SPW-Rs were also observed in our ischemic stroke model [18], in which synaptic input from entorhinal cortex to the dentate gyrus was affected due to cortical injury [31, 74].

Ample evidence supports a bidirectional relationship between diabetes mellitus (DM) and major depressive disorder (MDD) in humans [75-81]. Shared abnormal neurophysiological features between patients with DM and depression are well documented including elevated power in delta and theta bands, and impaired response to task-oriented stimulation such as increased P300 latency in EEG [82]. Interestingly, overlapping pathology such as the pattern of volumetric abnormality and neurocognitive deficits was also found between diabetic patients and those with depressive disorder [30]. Consistent with clinical evidence, depression-like behavior was detected in preclinical T2DM model db/db mice by forced swim test accompanied by thigmotaxis behavior and hypo-locomotion at a relatively young age of 10-11 weeks [83]. The role of impaired leptin production or signaling in depression was supported by a study in which treatment of diabetic mice with leptin reversed the depressive-like behavior in the tail suspension test [84]. However, the pharmacology and pathophysiology of leptin signaling defect in causing depression is not well understood. It is possible that leptin defect could cause depression by modulating the firing and downstream signaling of monoaminergic neurons in the forebrain. This is in line with the evidence that leptin receptor is expressed in the serotonergic raphe nuclei [85], and the leptin deficient ob/ob mice have reduced serotonin transporter expression in raphe nuclei [86]. Leptin also increased the production of forebrain 5-hydroxyindoleacetic acid, a breakdown product of serotonin [87]. In addition, systemic leptin treatment reversed the hedonic-like deficit induced by chronic stress and produced an antidepressant-like effect in the forced swim tests in rats [88]. Interestingly, the authors found that the targeted brain regions of leptin intervention are in the HPC and amygdala including the dentate gyrus as mapped by Fos expression [88].

Several limitations are noted in our study. First, LFP recording under anesthesia can potentially affect brain activity and may not fully mimic the natural state. However, urethane anesthesia not only preserves all the brain rhythms investigated in our study, but also induces spontaneous and rhythmic brain state alternations mimicking the natural sleep in mice and rats [89, 90], a state when sharp wave associated ripples occur, providing a stable and reproducible platform for the aged and diabetic mice in our study. Besides, it is well established that hippocampal theta rhythm recorded under urethane [91] is comparable to awake recording [92]. Furthermore, we were able to identify oscillation changes in multiple frequency ranges and alteration in network communication during acute and chronic stroke [17, 18], suggesting that recording under urethane anesthesia does not blunt the pathological changes in brain activity. Second, limited recording sites is one major weakness of our electrophysiology study, which precludes an in-depth analysis of the disrupted functional networks by age and T2DM. Although the linear array used in our study reveals superior hippocampal rhythms compared to conventional EEG, lacking globally distributed recording sites does limit our assessment of functional connectivity to only restricted cortical and hippocampal networks. Besides, without task or event-related recording, data collected under urethane anesthesia have limited implication in physiological cognitive function. Despite the compelling role of hippocampal neurogenesis in cognitive precision and maintaining the balance of excitation and inhibition within the DG-CA3 network, another main limitation of

our study is that we did not establish a causal relationship between reduced neurogenesis and perturbed electrophysiology in our T2DM model, which hinges upon future development of therapy to enhance or restore neurogenesis in the db/db mice.

Author Contributions

G.R. performed recordings, data analysis and contributed to the writing of the manuscript. Z.I. carried out data analysis and contributed to the writing of the manuscript. S.Z. performed data analysis validation. H.Z. contributed to neurogenesis analysis and the validation and plotting of electrophysiology results. Y.S. assisted in electrophysiology recording. A.Y. contributed to analysis methods and validated the analysis. J.L. conceived the study design, planning and supervision of the experiments, interpretation of results and writing of the manuscript. All authors have read and agreed to the published version of the manuscript.

Acknowledgements

This work was supported by NIH grant R01NS102886 (JL), R21NS120193 (JL), Research Career Scientist award IK6BX004600 (JL), the Eunice Kennedy Shiver National Institute of Child Health & Human Development of the National Institutes of Health under Award Number K12HD073945 (AY), and the Center for Neurotechnology (CNT, a National Science Foundation Engineering Research Center under Grant EEC-1028725) (AY). The authors would like to thank Dr. Charles Mcculoch for assisting with the statistical analysis.

Institutional Review Board Statement

The study was conducted in accordance with the Guide for Care and Use of Laboratory Animals issued by the National Institutes of Health and approved by San Francisco Veterans Affairs Medical Center Institutional Animal Care and Use Committee (protocol number 20-015, approved 8-10-2020).

Declaration of interest

The authors have no conflicts of interest to declare.

References

[1] Kaiser AB, Zhang N and Der Pluijm WV (2018). Global prevalence of type 2 diabetes over the next ten years (2018-2028). Diabetes, 67.

[2] van Sloten TT, Sedaghat S, Carnethon MR, Launer LJ and Stehouwer CD (2020). Cerebral microvascular complications of type 2 diabetes: stroke, cognitive dysfunction, and depression. The lancet Diabetes & endocrinology, 8: 325-36.

[3] Antal B, McMahon LP, Sultan SF, Lithen A, Wexler DJ, Dickerson B, et al. (2022). Type 2 diabetes mellitus accelerates brain aging and cognitive decline: Complementary findings from UK Biobank and meta-analyses. Elife, 11.

[4] Yu JH, Han K, Park S, Cho H, Kim J-W, Seo JA, et al. (2020). Incidence and risk factors for dementia in type 2 diabetes mellitus: a nationwide population-based study in Korea. Diabetes & metabolism journal, 44: 113-24.

[5] Dorsemans A-C, Couret D, Hoarau A, Meilhac O, Lefebvre d'Hellencourt C and Diotel N (2017). Diabetes, adult neurogenesis and brain remodeling: New insights from rodent and zebrafish models. Neurogenesis, 4: e1281862.

[6] Zhang H, Hao Y, Manor B, Novak P, Milberg W, Zhang J, et al. (2015). Intranasal insulin enhanced resting-state functional connectivity of hippocampal regions in type 2 diabetes. Diabetes, 64: 1025-34.

[7] Zhou H, Lu W, Shi Y, Bai F, Chang J, Yuan Y, et al. (2010). Impairments in cognition and resting-state connectivity of the hippocampus in elderly subjects with type 2 diabetes. Neuroscience letters, 473: 5-10.

[8] Benwell CSY, Davila-Perez P, Fried PJ, Jones RN, Travison TG, Santarnecchi E, et al. (2020). EEG spectral power abnormalities and their relationship with cognitive dysfunction in patients with Alzheimer's disease and type 2 diabetes. Neurobiol Aging, 85: 83-95.

[9] Dauwels J, Srinivasan K, Ramasubba Reddy M, Musha T, Vialatte F-B, Latchoumane C, et al. (2011). Slowing and loss of complexity in Alzheimer's EEG: two sides of the same coin? International journal of Alzheimer's disease, 2011.

[10] Zakaria ZZ, Ahmad MN and Qinna NA (2021). Animal Models in Type 2 Diabetes Mellitus Research: Pros and Cons. Jordan Journal of Agricultural Sciences, 17: 425-40.

[11] Berdugo-Vega G, Arias-Gil G, Lopez-Fernandez A, Artegiani B, Wasielewska JM, Lee CC, et al. (2020). Increasing neurogenesis refines hippocampal activity rejuvenating navigational learning strategies and contextual memory throughout life. Nat Commun, 11: 135.

[12] Leal SL and Yassa MA (2015). Neurocognitive Aging and the Hippocampus across Species. Trends Neurosci, 38: 800-12.

[13] Wilson IA, Gallagher M, Eichenbaum H and Tanila H (2006). Neurocognitive aging: prior memories hinder new hippocampal encoding. Trends Neurosci, 29: 662-70.

[14] Akamatsu Y, Nishijima Y, Lee CC, Yang SY, Shi L, An L, et al. (2015). Impaired leptomeningeal collateral flow contributes to the poor outcome following experimental stroke in the Type 2 diabetic mice. J Neurosci, 35: 3851-64.

[15] Kanoke A, Nishijima Y, Ljungberg M, Omodaka S, Yang SY, Wong S, et al. (2020). The effect of type 2 diabetes on CD36 expression and the uptake of oxLDL: Diabetes affects CD36 and oxLDL uptake. Exp Neurol, 334: 113461.

[16] Nishijima Y, Akamatsu Y, Yang SY, Lee CC, Baran U, Song S, et al. (2016). Impaired Collateral Flow Compensation During Chronic Cerebral Hypoperfusion in the Type 2 Diabetic Mice. Stroke, 47: 3014-21.

[17] He JW, Rabiller G, Nishijima Y, Akamatsu Y, Khateeb K, Yazdan-Shahmorad A, et al. (2020). Experimental cortical stroke induces aberrant increase of sharp-wave-associated ripples in the hippocampus and disrupts cortico-hippocampal communication. J Cereb Blood Flow Metab, 40: 1778-96.

[18] Ip Z, Rabiller G, He JW, Chavan S, Nishijima Y, Akamatsu Y, et al. (2021). Local field potentials identify features of cortico-hippocampal communication impacted by stroke and environmental enrichment therapy. J Neural Eng, 18.

[19] Laptinskaya D, Fissler P, Küster OC, Wischniowski J, Thurm F, Elbert T, et al. (2020). Global EEG coherence as a marker for cognition in older adults at risk for dementia. Psychophysiology, 57: e13515.

[20] Barth AM and Mody I (2011). Changes in hippocampal neuronal activity during and after unilateral selective hippocampal ischemia in vivo. J Neurosci, 31: 851-60.

[21] Lockmann AL, Laplagne DA, Leao RN and Tort AB (2016). A Respiration-Coupled Rhythm in the Rat Hippocampus Independent of Theta and Slow Oscillations. J Neurosci, 36: 5338-52.

[22] Wolansky T, Clement EA, Peters SR, Palczak MA and Dickson CT (2006). Hippocampal slow oscillation: a novel EEG state and its coordination with ongoing neocortical activity. J Neurosci, 26: 6213-29.

[23] Donoghue T, Haller M, Peterson EJ, Varma P, Sebastian P, Gao R, et al. (2020). Parameterizing neural power spectra into periodic and aperiodic components. Nat Neurosci, 23: 1655-65.

[24] Lanzone J, Colombo M, Sarasso S, Zappasodi F, Rosanova M, Massimini M, et al. (2022). EEG spectral exponent as a synthetic index for the longitudinal assessment of stroke recovery. Clinical Neurophysiology, 137: 92-101.

[25] Colombo MA, Napolitani M, Boly M, Gosseries O, Casarotto S, Rosanova M, et al. (2019). The spectral exponent of the resting EEG indexes the presence of consciousness during unresponsiveness induced by propofol, xenon, and ketamine. Neuroimage, 189: 631-44.

[26] Stam CJ, Nolte G and Daffertshofer A (2007). Phase lag index: assessment of functional connectivity from multi channel EEG and MEG with diminished bias from common sources. Hum Brain Mapp, 28: 1178-93.

[27] Vinck M, Oostenveld R, van Wingerden M, Battaglia F and Pennartz CM (2011). An improved index of phase-synchronization for electrophysiological data in the presence of volume-conduction, noise and sample-size bias. Neuroimage, 55: 1548-65.

[28] Bendat J and Piersol A (1986). Random data: Analysis and measurement procedures 2nd Edition A Wiley-Interscience Publication. New York.

[29] Tort AB, Komorowski R, Eichenbaum H and Kopell N (2010). Measuring phase-amplitude coupling between neuronal oscillations of different frequencies. J Neurophysiol, 104: 1195-210.

[30] McIntyre RS, Kenna HA, Nguyen HT, Law CW, Sultan F, Woldeyohannes HO, et al. (2010). Brain volume abnormalities and neurocognitive deficits in diabetes mellitus: points of pathophysiological commonality with mood disorders? Adv Ther, 27: 63-80.

[31] Sun C, Sun H, Wu S, Lee CC, Akamatsu Y, Wang RK, et al. (2013). Conditional ablation of neuroprogenitor cells in adult mice impedes recovery of poststroke cognitive function and reduces synaptic connectivity in the perforant pathway. J Neurosci, 33: 17314-25.

[32] Hong SM, Liu Z, Fan Y, Neumann M, Won SJ, Lac D, et al. (2007). Reduced hippocampal neurogenesis and skill reaching performance in adult Emx1 mutant mice. Exp Neurol, 206: 24-32.

[33] Liu Z, Fan Y, Won SJ, Neumann M, Hu D, Zhou L, et al. (2007). Chronic treatment with minocycline preserves adult new neurons and reduces functional impairment after focal cerebral ischemia. Stroke, 38: 146-52.

[34] Fan Y, Liu Z, Weinstein PR, Fike JR and Liu J (2007). Environmental enrichment enhances neurogenesis and improves functional outcome after cranial irradiation. Eur J Neurosci, 25: 38-46.

[35] Parent JM, Vexler ZS, Gong C, Derugin N and Ferriero DM (2002). Rat forebrain neurogenesis and striatal neuron replacement after focal stroke. Ann Neurol, 52: 802-13.

[36] Stendahl U, Willen H and Willen R (1979). Classification and grading of invasive squamous cell carcinoma of the uterine cervix. Acta Radiol Oncol Radiat Phys Biol, 18: 481-96.

[37] Giovanni A, Capone F, di Biase L, Ferreri F, Florio L, Guerra A, et al. (2017). Oscillatory Activities in Neurological Disorders of Elderly: Biomarkers to Target for Neuromodulation. Front Aging Neurosci, 9: 189.

[38] Marshall AC and Cooper NR (2017). The association between high levels of cumulative life stress and aberrant resting state EEG dynamics in old age. Biol Psychol, 127: 64-73.

[39] Neto E, Biessmann F, Aurlien H, Nordby H and Eichele T (2016). Regularized Linear Discriminant Analysis of EEG Features in Dementia Patients. Front Aging Neurosci, 8: 273.

[40] Rossini PM, Rossi S, Babiloni C and Polich J (2007). Clinical neurophysiology of aging brain: from normal aging to neurodegeneration. Prog Neurobiol, 83: 375-400.

[41] Vlahou EL, Thurm F, Kolassa IT and Schlee W (2014). Resting-state slow wave power, healthy aging and cognitive performance. Sci Rep, 4: 5101.

[42] Voytek B and Knight RT (2015). Dynamic network communication as a unifying neural basis for cognition,

development, aging, and disease. Biol Psychiatry, 77: 1089-97.
[43] Knyazeva MG, Barzegaran E, Vildavski VY and Demonet JF (2018). Aging of human alpha rhythm. Neurobiol Aging, 69: 261-73.
[44] Mierau A, Klimesch W and Lefebvre J (2017). State-dependent alpha peak frequency shifts: Experimental evidence, potential mechanisms and functional implications. Neuroscience, 360: 146-54.
[45] Hill AT, Clark GM, Bigelow FJ, Lum JA and Enticott PG (2022). Periodic and aperiodic neural activity displays age-dependent changes across early-to-middle childhood. Developmental Cognitive Neuroscience, 54: 101076.
[46] Gao R, Peterson EJ and Voytek B (2017). Inferring synaptic excitation/inhibition balance from field potentials. Neuroimage, 158: 70-78.
[47] Guo N, Soden ME, Herber C, Kim MT, Besnard A, Lin P, et al. (2018). Dentate granule cell recruitment of feedforward inhibition governs engram maintenance and remote memory generalization. Nat Med, 24: 438-49.
[48] Buzsáki G (2002). Theta oscillations in the hippocampus. Neuron, 33: 325-40.
[49] Zeng K, Wang Y, Ouyang G, Bian Z, Wang L and Li X (2015). Complex network analysis of resting state EEG in amnestic mild cognitive impairment patients with type 2 diabetes. Frontiers in Computational Neuroscience, 9: 133.
[50] Kuang Y, Wu Z, Xia R, Li X, Liu J, Dai Y, et al. (2022). Phase Lag Index of Resting-State EEG for Identification of Mild Cognitive Impairment Patients with Type 2 Diabetes. Brain Sci, 12.
[51] Youssef N, Xiao S, Liu M, Lian H, Li R, Chen X, et al. (2021). Functional Brain Networks in Mild Cognitive Impairment Based on Resting Electroencephalography Signals. Front Comput Neurosci, 15: 698386.
[52] Cassidy JM, Wodeyar A, Wu J, Kaur K, Masuda AK, Srinivasan R, et al. (2020). Low-frequency oscillations are a biomarker of injury and recovery after stroke. Stroke, 51: 1442-50.
[53] Khan DM, Masroor K, Jailani MFM, Yahya N, Yusoff MZ and Khan SM (2022). Development of wavelet coherence EEG as a biomarker for diagnosis of major depressive disorder. IEEE Sensors Journal, 22: 4315-25.
[54] Khan DM, Yahya N, Kamel N and Faye I (2023). A novel method for efficient estimation of brain effective connectivity in EEG. Comput Methods Programs Biomed, 228: 107242.
[55] Rodinskaia D, Radinski C and Labuhn J (2022). EEG coherence as a marker of functional connectivity disruption in Alzheimer's disease. Aging and Health Research, 2: 100098.
[56] Musaeus CS, Salem LC, Kjaer TW and Waldemar G (2021). Electroencephalographic functional connectivity is altered in persons with Down syndrome and Alzheimer's disease. J Intellect Disabil Res, 65: 236-45.
[57] Jacobson TK, Schmidt B, Hinman JR, Escabi MA and Markus EJ (2015). Age-related decrease in theta and gamma coherence across dorsal ca1 pyramidale and radiatum layers. Hippocampus, 25: 1327-35.
[58] Buzsaki G (2015). Hippocampal sharp wave-ripple: A cognitive biomarker for episodic memory and planning. Hippocampus, 25: 1073-188.
[59] Wang DX, Schmitt K, Seger S, Davila CE and Lega BC (2021). Cross-regional phase amplitude coupling supports the encoding of episodic memories. Hippocampus, 31: 481-92.
[60] Sun Q, Chen GQ, Wang XB, Yu Y, Hu YC, Yan LF, et al. (2018). Alterations of White Matter Integrity and Hippocampal Functional Connectivity in Type 2 Diabetes Without Mild Cognitive Impairment. Front Neuroanat, 12: 21.
[61] Liu D, Chen L, Duan S, Yin X, Yang W, Shi Y, et al. (2018). Disrupted balance of long-and short-range functional connectivity density in type 2 diabetes mellitus: a resting-state fMRI study. Frontiers in Neuroscience, 12: 875.
[62] Foster DJ (2017). Replay comes of age. Annual review of neuroscience, 40: 581-602.
[63] Oliva A, Fernández-Ruiz A, de Oliveira EF and Buzsáki G (2018). Origin of gamma frequency power during hippocampal sharp-wave ripples. Cell Reports, 25: 1693-700. e4.
[64] Kitanishi T, Ujita S, Fallahnezhad M, Kitanishi N, Ikegaya Y and Tashiro A (2015). Novelty-induced phase-locked firing to slow gamma oscillations in the hippocampus: requirement of synaptic plasticity. Neuron, 86: 1265-76.
[65] Fernandez-Ruiz A, Oliva A, Fermino de Oliveira E, Rocha-Almeida F, Tingley D and Buzsaki G (2019). Long-duration hippocampal sharp wave ripples improve memory. Science, 364: 1082-86.
[66] Fernández-Ruiz A, Oliva A, Soula M, Rocha-Almeida F, Nagy GA, Martin-Vazquez G, et al. (2021). Gamma rhythm communication between entorhinal cortex and dentate gyrus neuronal assemblies. Science, 372: eabf3119.
[67] Hollnagel J-O, Elzoheiry S, Gorgas K, Kins S, Beretta CA, Kirsch J, et al. (2019). Early alterations in hippocampal perisomatic GABAergic synapses and network oscillations in a mouse model of Alzheimer's disease amyloidosis. PloS one, 14: e0209228.
[68] Jadhav SP, Kemere C, German PW and Frank LM (2012). Awake hippocampal sharp-wave ripples support spatial memory. Science, 336: 1454-58.
[69] Jones EA, Gillespie AK, Yoon SY, Frank LM and Huang Y (2019). Early hippocampal sharp-wave ripple deficits predict later learning and memory impairments in an Alzheimer's disease mouse model. Cell reports, 29: 2123-33. e4.
[70] Le Van Quyen M, Staba R, Bragin A, Dickson C, Valderrama M, Fried I, et al. (2010). Large-scale microelectrode recordings of high-frequency gamma oscillations in human cortex during sleep. Journal of Neuroscience, 30: 7770-82.

[71] Luna VM, Anacker C, Burghardt NS, Khandaker H, Andreu V, Millette A, et al. (2019). Adult-born hippocampal neurons bidirectionally modulate entorhinal inputs into the dentate gyrus. Science, 364: 578-83.

[72] Oh MM, Simkin D and Disterhoft JF (2016). Intrinsic Hippocampal Excitability Changes of Opposite Signs and Different Origins in CA1 and CA3 Pyramidal Neurons Underlie Aging-Related Cognitive Deficits. Front Syst Neurosci, 10: 52.

[73] Cai X, Wei DS, Gallagher SE, Bagal A, Mei YA, Kao JP, et al. (2007). Hyperexcitability of distal dendrites in hippocampal pyramidal cells after chronic partial deafferentation. J Neurosci, 27: 59-68.

[74] Sato Y, Schmitt O, Ip Z, Rabiller G, Omodaka S, Tominaga T, et al. (2022). Pathological changes of brain oscillations following ischemic stroke. J Cereb Blood Flow Metab, 42: 1753-76.

[75] Kan C, Silva N, Golden SH, Rajala U, Timonen M, Stahl D, et al. (2013). A systematic review and meta-analysis of the association between depression and insulin resistance. Diabetes Care, 36: 480-9.

[76] Khaledi M, Haghighatdoost F, Feizi A and Aminorroaya A (2019). The prevalence of comorbid depression in patients with type 2 diabetes: an updated systematic review and meta-analysis on huge number of observational studies. Acta Diabetol, 56: 631-50.

[77] Lloyd CE, Pambianco G and Orchard TJ (2010). Does diabetes-related distress explain the presence of depressive symptoms and/or poor self-care in individuals with Type 1 diabetes? Diabet Med, 27: 234-7.

[78] Pan A, Lucas M, Sun Q, van Dam RM, Franco OH, Manson JE, et al. (2010). Bidirectional association between depression and type 2 diabetes mellitus in women. Arch Intern Med, 170: 1884-91.

[79] Zhu M, Li Y, Luo B, Cui J, Liu Y and Liu Y (2022). Comorbidity of Type 2 Diabetes Mellitus and Depression: Clinical Evidence and Rationale for the Exacerbation of Cardiovascular Disease. Front Cardiovasc Med, 9: 861110.

[80] Chien IC, Wu EL, Lin CH, Chou YJ and Chou P (2012). Prevalence of diabetes in patients with major depressive disorder: a population-based study. Compr Psychiatry, 53: 569-75.

[81] Demakakos P, Pierce MB and Hardy R (2010). Depressive symptoms and risk of type 2 diabetes in a national sample of middle-aged and older adults: the English longitudinal study of aging. Diabetes Care, 33: 792-7.

[82] Baskaran A, Milev R and McIntyre RS (2013). A review of electroencephalographic changes in diabetes mellitus in relation to major depressive disorder. Neuropsychiatr Dis Treat, 9: 143-50.

[83] Sharma AN, Elased KM, Garrett TL and Lucot JB (2010). Neurobehavioral deficits in db/db diabetic mice. Physiol Behav, 101: 381-8.

[84] Hirano S, Miyata S and Kamei J (2007). Antidepressant-like effect of leptin in streptozotocin-induced diabetic mice. Pharmacol Biochem Behav, 86: 27-31.

[85] Finn PD, Cunningham MJ, Rickard DG, Clifton DK and Steiner RA (2001). Serotonergic neurons are targets for leptin in the monkey. J Clin Endocrinol Metab, 86: 422-6.

[86] Collin M, Hakansson-Ovesjo ML, Misane I, Ogren SO and Meister B (2000). Decreased 5-HT transporter mRNA in neurons of the dorsal raphe nucleus and behavioral depression in the obese leptin-deficient ob/ob mouse. Brain Res Mol Brain Res, 81: 51-61.

[87] Calapai G, Corica F, Corsonello A, Sautebin L, Di Rosa M, Campo GM, et al. (1999). Leptin increases serotonin turnover by inhibition of brain nitric oxide synthesis. J Clin Invest, 104: 975-82.

[88] Lu XY, Kim CS, Frazer A and Zhang W (2006). Leptin: a potential novel antidepressant. Proc Natl Acad Sci U S A, 103: 1593-8.

[89] Suzuki SS and Smith GK (1988). Spontaneous EEG spikes in the normal hippocampus. V. Effects of ether, urethane, pentobarbital, atropine, diazepam and bicuculline. Electroencephalogr Clin Neurophysiol, 70: 84-95.

[90] Pagliardini S, Gosgnach S and Dickson CT (2013). Spontaneous sleep-like brain state alternations and breathing characteristics in urethane anesthetized mice. PLoS One, 8: e70411.

[91] Kramis R, Vanderwolf CH and Bland BH (1975). Two types of hippocampal rhythmical slow activity in both the rabbit and the rat: relations to behavior and effects of atropine, diethyl ether, urethane, and pentobarbital. Exp Neurol, 49: 58-85.

[92] Bland BH and Whishaw IQ (1976). Generators and topography of hippocampal theta (RSA) in the anaesthetized and freely moving rat. Brain Res, 118: 259-80.